CARBOCYANINE DYE ORIENTATION IN RED CELL MEMBRANE STUDIED BY MICROSCOPIC FLUORESCENCE POLARIZATION

DANIEL AXELROD, *Biophysics Research Division and Department of Physics, The University of Michigan, Ann Arbor, Michigan 48109 U.S.A*

ABSTRACT The orientation of an amphipathic, long acyl chain fluorescent carbocyanine dye [diI-C_{18}-(3)] in a biological membrane is examined by steady-state fluorescence polarization microscopy on portions of single erythrocyte ghosts. The thermodynamically plausible orientation model most consistent with the experimental data is one in which the diI-C_{18}-(3) conjugated bridge chromophore is parallel to the surface of the cell and the acyl chains are imbedded in the bilayer parallel to the phospholipid acyl chains. Comparison of the predictions of this model with the experimental data yields information on the intramolecular orientations of the dye's transition dipoles and on the dye's rate of rotation in the membrane around an axis normal to the membrane. To interpret the experimental data, formulae are derived to account for the effect of high aperture observation on fluorescence polarization ratios. These formulae are generally applicable to any high aperture polarization studies on microscopic samples, such as portions of single cells.

INTRODUCTION

Carbocyanine dyes are increasingly used as probes of membrane potential (1–3) and membrane lipid lateral mobility (4–7). The class of carbocyanine dyes with long hydrocarbon tails are particularly appealing as membrane probes because they are suggestive of phospholipids with their polar "head" groups and dual nonpolar acyl chains (Fig. 1). Because such lipid probes partition among regions of differing hydrophobicity in a chemically nonspecific manner, it is imperative to know their location and orientation in membranes to correctly interpret experimental observations. One would hope they orient in membranes parallel to the phospholipids in the bilayer. This orientation indeed appears to prevail in artificial planar bilayers, consisting of phospholipids (8) or oxidized cholesterol (9), as shown by fluorescence polarization studies. However, in biological cell membranes, where a significant amount of membrane protein and carbohydrate is present and the mode of dye incorporation into the cell membrane is poorly understood, one cannot immediately presume that carbocynanine dyes orient with their acyl chains parallel to those of the membrane bilayer phospholipids. Instead, it is plausible that the carbocyanine dye intercolates into "pockets" of integral or extrinsic protein molecules or forms vesicle-like structures adhering to the outside of the cell surface.

This paper reports upon steady-state fluorescence polarization measurements on microscopic subportions of single erythrocyte ghosts labeled with 3,3′-dioctadecylindocarbocyanine (diI-C_{18}-(3) or diI; Fig. 1) (1). Of the plausible models for diI orientation distribution in membranes, only the model in which diI's conjugated bridge lies in a plane parallel to the surface of the ghost is consistent with the experimental results. In view of the molecular

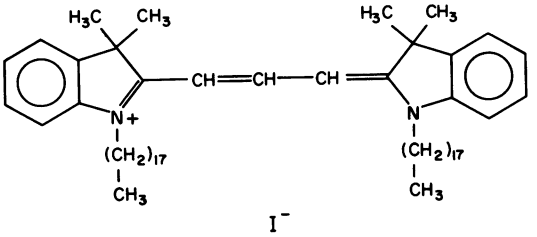

FIGURE 1 3,3′-Dioctadecylindocarbocyanine, diI-C_{18}-(3), abbreviated diI here.

structure of diI, this result strongly supports the view that diI is incorporated into the bilayer with its acyl chains roughly parallel to those of the bilayer phospholipids.

In addition to the diI results, a general theory for relating orientation distributions to fluorescence polarization intensities as observed by epi-illumination optics through high aperture objectives is presented in some detail. A similar theory based on a somewhat different approach has been independently derived by Dragsten (10) in his Ph.D. thesis. This theory should find application to any high aperture fluorescence polarization studies on microscopic samples, such as portions of single cells.

THEORY

In deriving a theory for the expected fluorescence polarization ratios of diI as observed by epi-illumination (i.e., a 180° angle between the central propagation directions of excitation and observed emission light) through a microscope, we must consider the following factors: *(a)* The rather wide solid angle of observation subtended by a high numerical aperture microscope objective; *(b)* A possibly nonzero angle between the absorption and emission dipoles of diI; *(c)* The particular orientation model to be tested, including the effect of rotational diffusion between the times of absorption and emission; *(d)* The observation of a finite source area containing a range of diI orientations, an effect which is particularly important when viewing tangentially at the edge of a cell; *(e)* The blurring effect of the optical resolution limit and the shallow depth of focus.

These factors are discussed sequentially in the following sections.

a. High Aperture Observation

The effect of high aperture observation on fluorescence polarization is discussed first without reference to any particular orientation distribution model because the results are generally applicable to any distribution of any fluorophore. A theory for this effect is presented by Dragsten in his Ph.D. thesis (10). Because of the relative inaccessibility of that work, an independently derived calculation employing a somewhat different approach is detailed in the Appendix. The main results are summarized in this section.

We excite the fluorescence by epi-illumination optics (i.e., through the objective) with polarized light. The objective collects the emitted fluorescence, which then passes through a polarizing analyzer filter oriented perpendicular ($\perp$) or parallel ($\parallel$) to the excitation polarization. We define a set X of right-handed coordinate axes such that the X_1 axis is parallel to the optical axis of the microscope and the X_3 axis is parallel to the electric field

vector of the polarized excitation light (Fig. 7, Appendix). A unit magnitude emission dipole in the sample has components (x_1, x_2, x_3) along these axes. As shown in the Appendix, the fluorescence intensities $I_\perp$ and $I_\parallel$ produced by this single dipole and observed through the analyzer filter can be expressed as:

$$I_\perp = K_a x_1^2 + K_c x_2^2 + K_b x_3^2$$
$$I_\parallel = K_a x_1^2 + K_b x_2^2 + K_c x_3^2, \tag{1}$$

where (suppressing common factors of π),

$$K_a = 1/3(2 - 3\cos\sigma_0 + \cos^3\sigma_0)$$
$$K_b = 1/12(1 - 3\cos\sigma_0 + 3\cos^2\sigma_0 - \cos^3\sigma_0)$$
$$K_c = 1/4(5 - 3\cos\sigma_0 - \cos^2\sigma_0 - \cos^3\sigma_0), \tag{2}$$

where σ_0 is the maximum half angle subtended by the objective as viewed from the sample. Angle σ_0 can be calculated from the known numerical aperture (N.A.) of the objective:

$$\text{N.A.} = n\sin\sigma_0, \tag{3}$$

where n is the index of refraction of the medium in which the sample is imbedded.

Nonzero factors K_a and K_b lead to the mixing in of fluorescence intensities from dipole moment components not normally observed at "zero" aperture, but important here due to the finite aperture's ability to "see around" the sample. For small σ_0 (the small aperture limit), $K_c \gg K_a, K_b$ as expected. Note that the only difference between $I_\perp$ and $I_\parallel$ is the reversal of K_b and K_c.

We now seek an expression for the fluorescence observed from an actual sample, which consists of a multitude of emission dipoles. First, we must consider the angular distribution of excited fluorescent molecules. The exact form of this distribution is a consequence of the anisotropic probability of excitation by polarized light, the distribution of molecular orientations in the sample, the angle between a molecule's absorption and emission dipole, and the rotation rate of an excited molecule. We denote this distribution by a weighting function $m(\Omega, \mu)$ where Ω abbreviates all the angular variables of the collection of molecules (i.e., the angles describing the anisotropic excitation and molecular orientations over which we will later integrate) and μ abbreviates all the constant parameters of each molecule (i.e., the angle between the transition dipoles, any fixed orientation angles over which we will not integrate, spatial location in the sample, and the molecular rotation rate). The total fluorescence is also proportional to the sample's size or extent, to be denoted here by a general variable s. Therefore, the total fluorescence $F_{\perp,\parallel}$ is:

$$F_{\perp,\parallel}(\mu) = \int_s \int_\Omega m(\Omega, \mu) I_{\perp,\parallel}\, d\Omega ds, \tag{4}$$

so that

$$F_\perp(\mu) = K_a J_1(\mu) + K_c J_2(\mu) + K_b J_3(\mu)$$
$$F_\parallel(\mu) = K_a J_1(\mu) + K_b J_2(\mu) + K_c J_3(\mu) \tag{5}$$

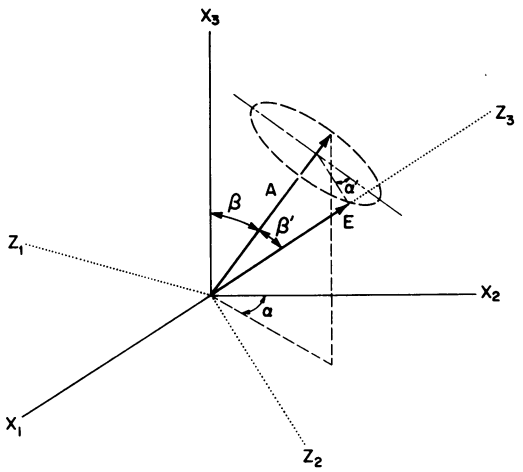

FIGURE 2 Polar angles β and β' and azimuthal angles α and α' of the absorption *(A)* and emission *(E)* dipoles, respectively. These angles are used in calculations concerning immobile, randomly oriented dil. In coordinate system Z, E is along Z_3, and Z_2 lies in the plane common to A and E. Angle α' is measured with respect to a diameter line lying in the plane of X_3 and A.

where

$$J_{i(\mu)} = \int_s \int_\Omega m(\Omega, \mu) x_i^2 \, d\Omega ds. \tag{6}$$

We always normalize $d\Omega$ so that $\int_\Omega d\Omega = 1$.

The form of Eqs. 4–6 emphasizes the generality of the aperture-dependent K factors: the set of K values is a property only of the optical system whereas the set of J values is a property only of the sample.

We now proceed to apply the general formulae of this section to the particular distributions $m(\Omega, \mu)$ of interest here.

b. Angle between Absorption and Emission Dipoles

Information about the angle between the absorption and emission dipoles of dil can be obtained from polarization measurements on a sample in which dil is immobile and randomly oriented. To compute the J_i integrals for this case, we define angles in the X coordinate system as shown in Fig. 2. In this figure, α and β are the azimuthal and polar angles of the absorption dipole with respect to the X_3 axis, and α' and β' are the azimuthal and polar angles of the emission dipole with respect to the direction of the absorption dipole.

To find the components of the emission dipole (x_1, x_2, x_3) along the X_i axes, we first define a coordinate system Z in which the emission dipole has components (0, 0, 1). We choose the Z_2 axis of this system to lie in the plane of the emission dipole E and the absorption dipole A. We then transform from this emission dipole-fixed Z system back to the laboratory-fixed X system by four successive rotations:[1] (1) angle β' around the Z_1 axis; (2) angle α' around the

[1]Rotations appearing counterclockwise as viewed from the positive rotation axis toward the origin are considered positive.

new Z_3 axis; (3) angle β around the newest Z_1 axis; and (4) angle α around the newest Z_3 axis. The result is:

$$x_1 = \cos\alpha \sin\alpha' \sin\beta' + \sin\alpha \cos\beta \cos\alpha' \sin\beta' + \sin\alpha \sin\beta \cos\beta'$$
$$x_2 = -\sin\alpha \sin\alpha' \sin\beta' + \cos\alpha \cos\beta \cos\alpha' \sin\beta' + \cos\alpha \sin\beta \cos\beta'$$
$$x_3 = -\sin\beta \cos\alpha' \sin\beta' + \cos\beta \cos\beta'. \tag{7}$$

The weighting function $m(\Omega, \mu)$ for excited molecules in this system is simply

$$m(\Omega, \mu) = \cos^2\beta. \tag{8}$$

Here Ω represents variables β, α, and α', and μ represents parameter β', the angle between the absorption and emission dipoles.

Finally, we note that the normalized differential of Eq. 6 is

$$d\Omega = (1/8\pi^2) \sin\beta d\beta d\alpha d\alpha'. \tag{9}$$

Combining Eqs. 7–9 into Eq. 6, we find:

$$J_1 = (1/15)(\sin^2\beta' + 1)$$
$$J_2 = (1/15)(\sin^2\beta' + 1)$$
$$J_3 = (1/15)(3 - 2\sin^2\beta'). \tag{10}$$

The integration over spatial variable s will only lead to a constant multiplicative factor here and has been suppressed..

By substituting Eqs. 10 into Eqs. 5, we can find $F_\perp(\beta')/F_\parallel(\beta')$, thereby allowing calculation of β', given an experimentally measured $F_\perp/F_\parallel$. For $\beta' = 0$ in the limit of small aperture, $F_\perp/F_\parallel = 1/3$, as expected (11) for a random orientation distribution. In the case of dil, however, the situation is a little more complicated, as can be seen with reference to Fig. 3. Because of the symmetry of the dil fluorophore, both the absorption and emission dipoles must have mirror-image pairs, each making angles of $\pm\theta$ and $\pm\theta'$ with the direction of the conjugated bridge, respectively. Therefore, angle β' may be either $\beta'_+ \equiv \theta + \theta'$ or $\beta'_- \equiv \theta - \theta'$

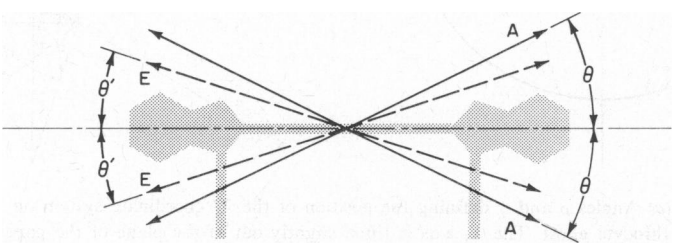

FIGURE 3 Definition of angles θ and θ' of adsorption *(A)* and emission *(E)* dipoles, respectively, relative to the dil molecular structure (shaded).

with equal probability. The fluorescence is then:

$$F_{\perp,\parallel} = \tfrac{1}{2}[F_{\perp,\parallel}(\beta'_+) + F_{\perp,\parallel}(\beta')]. \tag{11}$$

Given an experimentally measured $F_\perp / F_\parallel$, we can calculate θ' if we know θ independently (or vice-versa).

c. Model for dil Orientation and Rotational Motion in Membranes

We are now ready to postulate a reasonable model for dil orientation in membranes. We propose that dil's conjugated bridge is parallel to the phospholipid bilayer surface with hydrocarbon tails extending normal to the surface. We furthermore assume that dil is free to rotate around its symmetry axis normal to the surface.

Fig. 4 *a* illustrates the coordinate system to be used in the following analysis. Assuming that X_1 axis (i.e., the optical axis) is the "north-south" axis of a spherical erythrocyte ghost, then any point on the surface is described by a "latitude" angle γ and a "longitude" angle ρ. Longitude $\rho = 0$ is set where the positive X_3 axis (i.e., the excitation polarization direction) intersects the equator.

We can most easily express the components of excitation and emission dipoles along a coordinate system X' fixed with respect to a normal to the surface, as shown in Fig. 4 *a*. The rotation matrix transforming coordinates from the X' system to the X system is formed from the product of two successive rotations: a rotation of angle $-\gamma$ around X'_2, followed by a rotation of angle ρ around the new X'_1. Angles η and η' are the amounts of rotation of the dil absorption and emission dipoles, respectively, around the X'_3 axis normal to the surface (Fig. 4 *b*). In the X' system, the components of an emission dipole are ($\cos\theta' \sin\eta'$, $\cos\theta' \cos\eta'$,

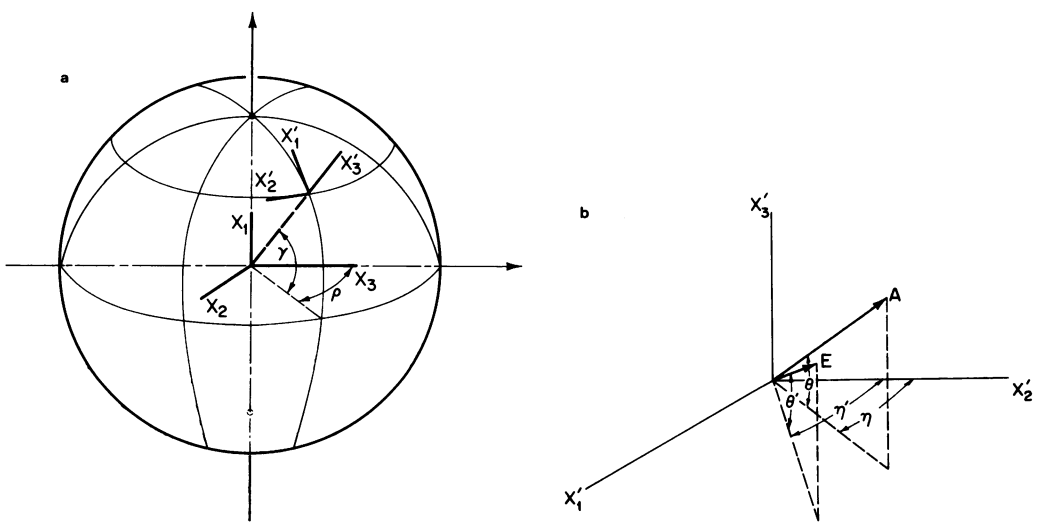

FIGURE 4 *(a)* Angles ρ and γ defining the position of the X' coordinate system on the surface of a spherical erythrocyte ghost. The X_1 axis is tilted slightly out of the plane of the paper for clarity. *(b)* Absorption *(A)* and emission *(E)* dipole moment vectors with respect to the surface-fixed X' system. As both *A* and *E* lie in the plane of the dil conjugated rings, then $\eta \neq \eta'$ implies a tilt of the dil conjugated ring system away from orthogonality with the cell surface ($X'_1 - X'_2$) plane.

sin θ'); the components of an absorption dipole are similar, except that unprimed θ and η are substituted for θ' and η'. Transformed into the optical-axis fixed X system, the emission dipole moment components are:

$$x_1 = \cos\gamma\cos\theta'\sin\eta' - \sin\gamma\sin\theta'$$

$$x_2 = \sin\gamma\sin\rho\cos\theta'\sin\eta' + \cos\rho\cos\theta'\cos\eta' + \cos\gamma\sin\rho\sin\theta'$$

$$x_3 = \sin\dot{\gamma}\cos\rho\cos\theta'\sin\eta' - \sin\rho\cos\theta'\cos\eta' + \cos\gamma\cos\rho\sin\theta'. \quad (12)$$

As before, the absorption dipole moment components are obtained by substituting θ and η for θ' and η'. Eqs. 12 are analogous to Eqs. 7 except that new angles have been defined for convenience in our proposed model of diI:membrane orientation distribution.

We wish to take into account any diffusional rotation of diI around the X_3' axis between the times of absorption and emission. Rotational diffusion affects the excited molecule orientation density $m(\Omega, \mu)$. Given that a molecule is at orientation angle η_0 when it absorbs a photon, and orientation angle η at a time Δt later when it emits a photon, then

$$m(\Omega, \mu) = \frac{1}{\tau}\int_{\eta_0=-\pi}^{\pi}\int_{\Delta t=0}^{\infty}\cos^2\beta_0 p(\Delta\eta, \Delta t)e^{-\Delta t/\tau}\,d\eta_0 d\Delta t, \quad (13)$$

where $\tau \cong$ the fluorescence lifetime, and $\Delta\eta \equiv \eta - \eta_0$. General variable Ω here represents η and general constant parameter μ represents θ, ρ, and γ. Angle β_0 is the angle between the absorption dipole and the excitation light polarization direction at the time of absorption ($\Delta t = 0$). The $\cos^2\beta_0$ term of Eq. 13 is just the square of the expression x_3 of Eq. 12 with θ' and η' replaced by θ and η_0.

The probability density function $p(\Delta\eta, \Delta t)$ is the solution of the rotational diffusion equation:

$$(1/D)(\partial p/\partial\Delta t) = (\partial^2 p/\partial\Delta\eta^2), \quad (14)$$

with the delta-function initial condition $p(\Delta\eta, 0) = \delta(\Delta\eta)(\text{mod } 2\pi)$ and $D =$ the rotational diffusion constant. The solution is:

$$p(\Delta\eta, \Delta t) = \frac{1}{2\pi} + \frac{1}{\pi}\sum_{k=1}^{\infty} e^{-k^2 D\Delta t}\cos k\Delta\eta. \quad (15)$$

We explicitly evaluate the integral of Eq. 13 along two longitudinal lines on the ghost surface at which we will make experimental measurements: $\rho = 0$ and $\rho = (\pi/2)$. The results are:

$$m_{\rho=0} = \frac{1}{2}\sin^2\gamma\cos^2\theta + \cos^2\gamma\sin^2\theta + \frac{\cos 2\eta\sin^2\gamma\cos^2\theta}{2(4D\tau + 1)} - [2\cos\eta/(D\tau + 1)]\sin\gamma\cos\gamma\sin\theta\cos\theta \quad (16)$$

$$m_{\rho=\pi/2} = \frac{1}{2}\cos^2\theta\left(1 - \frac{\cos 2\eta}{4D\tau + 1}\right). \quad (17)$$

d. Finite Size Observation Area

We may now evaluate the J_i's using Eq. 6. We are particularly interested in measuring the fluorescence polarization in three regions on the microscope image of the erythrocyte ghost

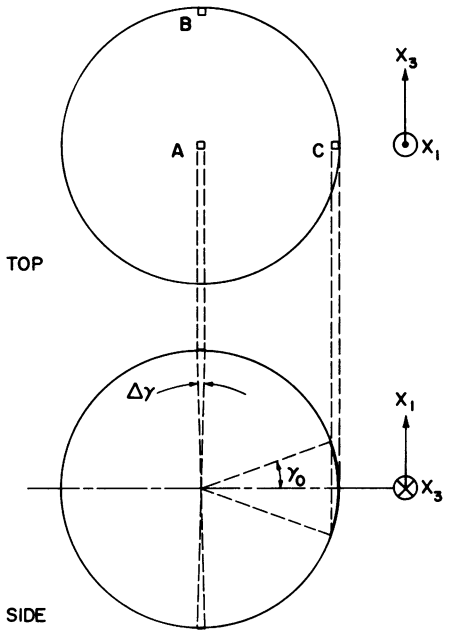

FIGURE 5 Two schematic views of the erythrocyte ghost. The "top" view looks along the optical axis X_1, and shows the location of observation regions *A*, *B*, and *C*. The "side" view looks along the excitation polarization axis X_3 and shows the angles $\Delta\gamma$ and γ_0 subtended by the observation regions at the middle and edge of the ghost, respectively. The area of an observation region relative to the erythrocyte ghost image area as illustrated here is approximately the same as experimentally employed in this study.

(Fig. 5): *(A)* the middle of the image at $\gamma = (\pi/2)$; *(B)* the edge region at $\rho = 0$; and *(C)* the edge region at $\rho = \pm(\pi/2)$. We observe each of these regions through a small square aperture placed in an image plane of the microscope. At the middle of the ghost, the aperture permits viewing of an angle $\Delta\gamma$ around $\gamma = \pm(\pi/2)$, where $\Delta\gamma \ll (\pi/2)$. At the edge of the ghost, however, the aperture permits viewing of a much larger angle, ranging from $-\gamma_0$ to $+\gamma_0$. In this light collection geometry, the infinitesmal ds of Eq. 6 corresponds to $d\gamma$, and we integrate γ over its relevant range for the middle or edge of the ghost. The infinitesmal $d\Omega = (1/2\pi)d\eta$, and we integrate η from $-\pi$ to π. Note that variable η' that appears in Eqs. 12 is not independent because $\eta' - \eta(\equiv\psi)$ is a constant related to the tilt angle between dil's conjugated plane and the normal to the ghost surface (see Fig. 4 *b*).

The results of these integrations are shown below for each of the three observation regions:

A. MIDDLE $\left(\Delta\gamma \text{ region around } \gamma = \pm\frac{\pi}{2}\right)$

$$J_1 = \Delta\gamma \cos^2\theta \sin^2\theta'$$

$$J_2 = \frac{1}{2}\Delta\gamma \cos^2\theta \cos^2\theta'\left[1 - \frac{\cos 2\psi}{2(4D\tau + 1)}\right]$$

$$J_3 = \frac{1}{2}\Delta\gamma \cos^2\theta \cos^2\theta'\left[1 + \frac{\cos 2\psi}{2(4D\tau + 1)}\right]. \qquad (18)$$

B. EDGE ($\rho = 0, -\gamma_0 < \gamma < \gamma_0$)

$$J_1 = \frac{T}{4}\cos^2\theta\cos^2\theta'\left[1 + \frac{\cos 2\psi}{2(4D\tau + 1)}\right] + \frac{V}{2}\sin^2\theta\cos^2\theta' + \frac{U}{2}\cos^2\theta\sin^2\theta'$$
$$+ T\sin^2\theta\sin^2\theta' - \frac{2T}{D\tau + 1}\cos\theta\sin\theta\cos\theta'\sin\theta'\cos\psi$$

$$J_2 = \frac{S}{4}\cos^2\theta\cos^2\theta'\left[1 - \frac{\cos 2\psi}{2(4D\tau + 1)}\right] + \frac{R}{2}\sin^2\theta\cos^2\theta'$$

$$J_3 = \frac{U}{4}\cos^2\theta\cos^2\theta'\left[1 + \frac{\cos 2\psi}{2(4D\tau + 1)}\right] + \frac{T}{2}\sin^2\theta\cos^2\theta' + \frac{T}{2}\cos^2\theta\sin^2\theta'$$
$$+ V\sin^2\theta\sin^2\theta' + \frac{2T}{D\tau + 1}\cos\theta\sin\theta\cos\theta'\sin\theta'\cos\psi. \quad (19)$$

C. EDGE ($\rho = (\pi/2), -\gamma_0 < \gamma < \gamma_0$)

$$J_1 = \frac{R}{4}\cos^2\theta\cos^2\theta'\left[1 - \frac{\cos 2\psi}{2(4D\tau + 1)}\right] + \frac{S}{2}\cos^2\theta\sin^2\theta'$$

$$J_2 = \frac{S}{4}\cos^2\theta\cos^2\theta'\left[1 - \frac{\cos 2\psi}{2(4D\tau + 1)}\right] + \frac{R}{2}\cos^2\theta\sin^2\theta'$$

$$J_3 = \frac{\gamma_0}{2}\cos^2\theta\cos^2\theta'\left[1 + \frac{\cos 2\psi}{2(4D\tau + 1)}\right]. \quad (20)$$

Factors R-V represent the following functions of γ_0:

$$R \equiv \gamma_0 + (1/2)\sin 2\gamma_0$$
$$S \equiv \gamma_0 - (1/2)\sin 2\gamma_0$$
$$T \equiv (1/4)[\gamma_0 - (1/4)\sin 2\gamma_0]$$
$$U \equiv \frac{1}{2}\left(\frac{3\gamma_0}{2} - \sin 2\gamma_0 + \frac{\sin 4\gamma_0}{8}\right)$$
$$V \equiv \frac{1}{2}\left(\frac{3\gamma_0}{2} + \sin 2\gamma_0 + \frac{\sin 4\gamma_0}{8}\right). \quad (21)$$

By using these equations for J_i, the fluorescence intensities $F_\perp$ and $F_\parallel$ for each of the three regions can be calculated from Eqs. 5. But in view of the arguments leading to Eq. 11, we must average the $F_{\perp,\parallel}$ calculated for the two pairs of angles (θ, θ') and $(\theta, -\theta')$. The fluorescence intensities will be notated by $F^A_{\perp,\parallel}$, $F^B_{\perp,\parallel}$, and $F^C_{\perp,\parallel}$ for each of the three regions A, B, and C, respectively.

e. Optical Resolution and Focusing Limit

Because of the blurring effect of the optical resolution limit, the edge of the ghost appears "fuzzy." Positioning the square observation aperture then becomes somewhat difficult

experimentally. Assuming it is positioned to optimally collect light from the edge region, the aperture will extend past the geometrical image of the edge. Light originating from $|\gamma| \leq \gamma_0$ will be collected with less efficiency than would be expected from the geometrical optics considerations of the last section, and light from $|\gamma| > \gamma_0$ may contribute to the total intensity. Therefore, neither the uniform weighting of contributions from different γ implied in the γ integration of the last section nor the sharp $\pm\gamma_0$ integration limits are precisely correct.

Although absolute edge fluorescence intensities are sensitive functions of γ_0, polarization ratios among edge fluorescence intensities are more slowly varying functions of γ_0 and therefore rather insensitive to resolution limit blurring. The main error due to the resolution limit arises in the ratio between fluorescence intensities at the edge with those at the middle of the ghost image. The error in this type of ratio can be estimated by convoluting the intensity of light expected from each γ with a blurring function approximated from diffraction theory.[2] For the 1.25 numerical aperture objective used in these experiments, the error is an underestimate of about 25% in the theoretical ratio $F_{\parallel}^{A}/F_{\parallel}^{C}$; an appropriate correction factor is therefore applied to the theoretical ratio before comparison with experimental results.

Blurring due to the finite depth of focus has not been taken into account in the theory but should give rise to minor contributions from $|\gamma| > \gamma_0$ and slightly reduced contributions from $|\gamma| \leq \gamma_0$ at edge regions. As with the resolution limit, this kind of blurring will not greatly affect polarization ratios among edge measurements, but will lead to a slight underestimate of $F_{\parallel}^{A}/F_{\parallel}^{C}$.

EXPERIMENTAL METHODS

Labeling of Erythrocyte Membranes

One drop of fresh human blood is added to 0.5 ml of Hank's Balanced Salt Solution (HBSS) (Grand Island Biological Co., Grand Island, N.Y.) containing 2.5 μl of 0.3 mg/ml diI in ethanol. The mixture is incubated for 15 min at 37°. DiI labeling of erythrocytes occurs without causing them to hemolyze. 5 ml of distilled water is then added, thereby hemolyzing the erythrocytes. Centrifugation at 5000 *g* for 30 min and removal of the supernatant is followed by resuspension of the ghosts in 1 ml HBSS containing 1 mg/ml of bovine serum albumin. A drop of this ghost suspension is placed on a poly-*L*-lysine precoated glass coverslip. After 1 h to allow for settling, the spherical ghosts are viewed in an inverted fluorescence miscroscope (Leitz Diavert; E. Leitz Inc., Rockleigh, N.J.).

The amount of diI incorporated into erythrocytes by this technique varies greatly from cell to cell in the same sample. Generally, the more brightly labeled cells were chosen for this polarization study.

DiI is completely insoluble in water and no diI fluorescence is ever seen inside the volume of a ghost.

Preparation of Immobile, Randomly Oriented diI

Twenty μl of 0.3 mg/ml diI in ethanol is dissolved in 0.5 ml of clear colorless encapsulating resin (Dow-Corning Corp., Midland, Mich.; Sylgard 182) and allowed to set overnight at 60° on a polished surface. The encapsulating resin is then peeled off the surface, resulting in a smooth, 0.2-mm thick sheet of highly fluorescent, clear, colored plastic, the fluorescence of which is almost entirely due to encapsulated diI.

---

[2]The diffraction pattern of a circular hole (corresponding to the pupil of the objective) is a rather unwieldy function for this calculation. For simplicity, the blurring function instead is chosen to be the single slit diffraction function $\sin^2 ax/(ax)^2$ where a is chosen so that the distance from the central maximum to the first node is equal to the resolution of the objective ($=0.61\lambda$/numerical aperture). The use of a slit rather than a circular hole pattern is not expected to alter the conclusions significantly.

Optics and Electronics

The fluorescence of the sample is excited with 514.5-nm line of an argon laser (Lexel Corp., Palo Alto, Calif.; model 95-3) by epi-illumination (i.e., reflection by a dichroic mirror) through the objective of the microscope, with the illumination defocused to cover the whole field of view. The laser light is highly polarized by intracavity Brewster angle windows; no polarizing filters are necessary in the excitation beam. The laser intensity is sufficiently stable ($\pm 1\%$) for these experiments without any special normalization procedures. The laser light is sufficiently attenuated to avoid significant photobleaching during measurements. Fluorescence is collected at 180° with respect to the incident beam by a 100 ×, 1.25 numerical aperture oil immersion objective for erythrocyte ghost experiments, or a 10 ×, 0.25 numerical aperture air objective for the immobilized dil experiments. The dichroic mirror and a colored glass filter blocks scattered excitation light. Fluorescence light then passes through a polarizing filter (Polaroid Corp., Cambridge, Mass.; HN 32; 0.010-in thickness) mounted on a two-position slider and oriented with its transmission axis either parallel or perpendicular to the excitation light polarization direction. At a real image plane of the microscope, the light passes through a centerable rectangular diaphragm adjusted in size to correspond to a 0.25 × 0.25-μm square on the microscope image. (The diaphragm and the mechanism for viewing its size and position are part of the Leitz MPV-1 photometer unit; E. Leitz Inc.) Light is detected by an RCA C31034A photomultiplier tube (RCA Electro Optics, Lancaster, Pa.), thermoelectrically cooled to −30°. The anode output of the photomultiplier is photon-counted and converted to an analog signal for plotting on a strip chart recorder.

A constant systematic polarization introduced by the microscope epi-illumination and photometer systems was detected, and all experimental results are appropriately corrected for it. The magnitude of this correction was found by measuring the response of the microscope/photometer system to equal intensity illumination of each orthogonal polarization as viewed through a 10 × objective. The light source for this experiment was the completely unpolarized tungsten filament/diffusing screen combination of the mirror-free transmitted illumination source of the Leitz Diavert (E. Leitz Inc.), in series with a rotatable polarizing filter.

Several experiments that might reveal strain birefringence in the encapsulating resin used for immobilized dil experiments were performed and no significant birefringence was found. Firstly, introduction of a sheet of polymerized resin in front of the objective did not alter the measurements of systematic polarization, as described above. Also, the measured fluorescence polarization ratios of dil in the encapsulating resin sheet were constant to within 2% over many readings of varying location, sheet thickness, and sheet orientation.

EXPERIMENTAL RESULTS AND DISCUSSION

In comparing the theoretical predictions of the proposed orientation model with experimental results on ghosts, we note that there are five independent experimental parameters ($F^A_\perp/F^A_\parallel$, $F^B_\perp/F^B_\parallel$, $F^C_\perp/F^C_\parallel$, $F^A_\parallel/F^C_\parallel$, $F^B_\parallel/F^C_\parallel$), and four "adjustable" theoretical parameters (D_T, θ, ψ, and γ_0). Of these latter four, two are not "freely" adjustable: ψ, related to the tilt angle of the conjugated ring system with respect to the plane of the acyl chains, is likely to be close to zero; and γ_0, the half angle subtended by the square image plane aperture around the edge of the ghost, must be close to the value predicted by geometrical optics and resolution considerations. Once θ and ψ are chosen, θ' is determined by the experimental results on dil immobilized in encapsulating resin. Therefore, there are ample experimental results relative to adjustable theoretical parameters to nontrivially test the proposed orientation model.

Figs. 6 *a* and *b* are fluorescence photographs of dil-labeled erythrocyte ghosts, viewed through an analyzer filter oriented parallel and perpendicular, respectively, to the excitation polarization direction. The fluorescence is clearly polarized and the intensity variation around the ghost's edge is pronounced, in a manner qualitatively expected from the proposed model.

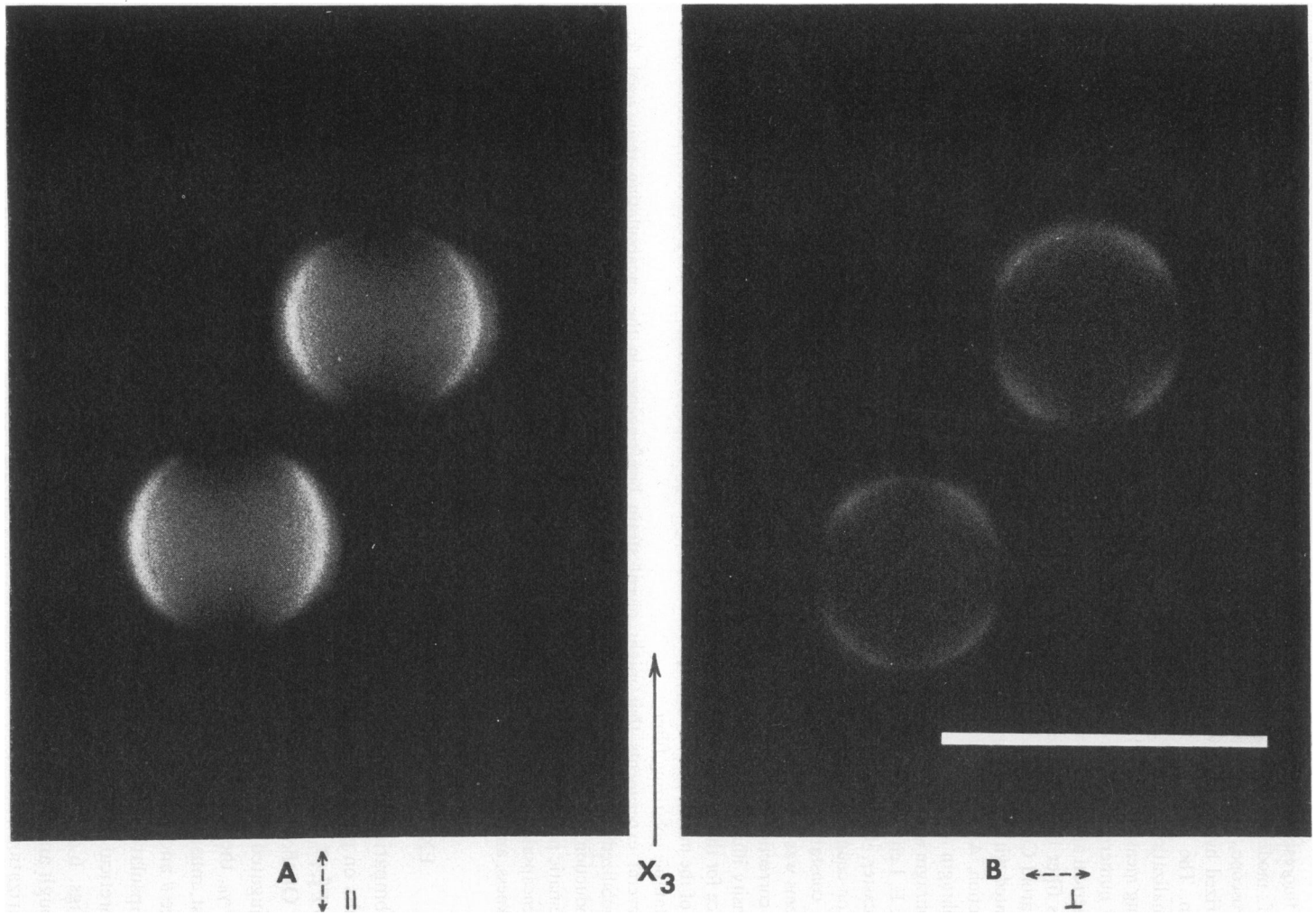

FIGURE 6 Fluorescence photographs of diI-labeled erythrocyte ghosts. The polarizing analyzer is oriented *(a)* parallel, and *(b)* perpendicular to the excitation polarization direction, which is denoted by an arrow. Scale bar = 10 μm. Tri-X film (Eastman Kodak Co., Rochester, N.Y.) developed at ASA 3000.

TABLE I

diI FLUORESCENCE POLARIZATION IN GHOSTS AND IN ENCAPSULATING RESIN: THEORY VS. EXPERIMENT

Polarization Ratio	Theory		Experiment
	100% Oriented	88% Oriented	
$F_\perp^A/F_\parallel^A$	0.63	0.62	0.72 ± 0.06
$F_\perp^B/F_\parallel^B$	3.3	2.3	1.8 ± 0.3
$F_\perp^C/F_\parallel^C$	0.21	0.24	0.22 ± 0.05
$F_\parallel^A/F_\parallel^C$	0.32	0.40	0.38 ± 0.05
$F_\parallel^B/F_\parallel^C$	0.16	0.22	0.17 ± 0.05
$F_\perp/F_\parallel$*	0.48		0.48 ± 0.01

*Immobile, randomly oriented diI in encapsulating resin.

Parameters chosen: $\gamma = 17.2°$, $\Delta\gamma = 4.9°$, $\psi = 0°$, $\theta = 28°$, $\theta' = 0°$, and $D_T = 0.27$.

Comparison of the experimentally measured polarization ratios with the theoretical predictions of two variations of the proposed model. In one variation, 100% of the diI conjugated bridges are assumed to lie parallel to the membrane; in the other variation, 88% of the bridges are assumed to have this orientation, with the remaining 12% randomly oriented. The experimental data on ghosts is an average of five different cells, with standard deviations as indicated. The parameters chosen for the theoretical computations are listed. Parameter $\Delta\gamma$ is the angle subtended by a 0.25-μm side square aperture image on a 2.9-μm radius spherical erythrocyte at the middle (i.e., observation region *A*). Parameter γ_0 is chosen to be consistent with the 0.25-μm aperture image and the blurring effects of the resolution limit at the ghost edge (regions *B* and *C*).

Table I compares the theoretical and experimental results for the five independent polarization ratios, using the particular set of parameters listed in the table caption. The agreement is quite satisfactory, with the possible exception of $F_\perp^B/F_\parallel^B$. The parameters selected are physically and optically quite reasonable; significant alteration in the set of parameters tends to make the agreement worse. One can regard these values of D_T, θ, θ', and ψ as an extra bonus, because they contain information about diI's motion and intramolecular transition dipole orientations which was not previously known or assumed in the theory. However, these values are probably only rough approximations to the truth because the theoretical results are not very sensitive to variations in some of the parameters and the experimental values upon which they are based have significant standard deviations. Agreement in the ratio $F_\parallel^A/F_\parallel^C$, although entirely satisfactory, should not be considered as stringent a test of the model as other ratios because of the reasons discussed in the Theory section *e*.

Perhaps the agreement error in $F_\perp^B/F_\parallel^B$ contains an important message. The error cannot be eliminated by adjusting parameters without introducing an even more serious disagreement in other ratios. The difficulty is that $F_\perp^B/F_\parallel^B$ is a ratio between two quite small fluorescence intensities in an edge region only weakly excited by the incident light. Fluorescence from small amounts of diI in a less well-ordered orientation than the postulated model could contribute significantly to the very small $F_\parallel^B$ and thereby reduce the expected $F_\perp^B/F_\parallel^B$ toward the experimental value.

The effect on all the ratios of a small fraction of randomly oriented diI in the membrane has actually been calculated quantitatively, by using Eqs. 10 for the random component and Eqs. 18–21 for the oriented component. (Eqs. 10 must be explicitly multiplied by the spatial factor $\int_s ds$ here, which is $2\Delta\gamma$ for the middle region *A* and $2\gamma_0$ for the edge regions *B* and *C*). Table I shows the results of such a calculation, assuming that 12% of all the diI in the membrane is

completely randomly oriented and the other 88% follows the oriented model postulated here. In this case, agreement between theory and experiment is reasonably good for all of the ratios, including $F_{\perp}^{B}/F_{\parallel}^{B}$.

The choice of 12% for the fraction of random dil is especially appealing because FPR measurements (5–7) consistently show that 5–15% of dil in biological membranes is relatively laterally immobile. Perhaps this 12% component consists of dil bound or intercolated into almost immobile membrane proteins (12) wherein it acquires both a less ordered orientation distribution and a much reduced lateral mobility. On the other hand, 85–95% of the dil has a lateral mobility at least three orders of magnitude faster than the upper bound for protein motion in erythrocyte membrane.[3] It would seem reasonable to associate this large mobile fraction with the dominant (88%) highly oriented dil component. (The high lateral mobility of this component also argues against any disorientation of the acyl chains of this class of dil molecules induced by strong interaction with membrane proteins.)

Numerous dil polarization measurements have also been performed on nonhemolyzed dil-labeled erythrocytes. The results are entirely consistent with those reported here for ghosts. The dil concentration (as estimated by total fluorescence) of the cells chosen for the nonhemolyzed erythrocyte experiments ranged over an order of magnitude. No dependence of polarization ratios on dil concentration was observed, which argues against dil-dil collisional energy transfer affecting the observed polarizations.

Other less-ordered orientation models seem thermodynamically plausible, such as surface-adhering, vesicle-like structures of dil or intercolation of dil into cell surface proteins. However, such models would clearly predict a more uniform fluorescence intensity around the ghost edge and a lower fluorescence polarization in maximally excited regions than actually observed or predicted by our proposed model.

The experimental results are consistent with a model in which the great majority of the dil conjugated bridges lie "parallel" to the surface. But how much nonparallelism or "wobble" can the experimental results accomodate? To answer this without deriving formulae for an entirely new model, we can alter the parallelism in a well-defined manner within the framework of the present model and see how the polarization ratios are affected. It is most convenient to postulate that the bridge of each dil makes an angle of θ_0 with the surface but still rotates around an axis normal to the surface. We can still use Eqs. 18–21 to calculate the J values, except that the former averaging of results for the two pairs of angles $(\theta, \pm\theta')$ now becomes an average of J values for the four pairs of angles $(\theta_0 \pm \theta, \theta_0 \pm \theta')$. These four pairs represent all the equiprobable sets of angles made by the absorption and emission dipoles with the cell surface. Intramolecular angles θ and θ' are chosen, as before, to satisfy the experimental results for randomly oriented immobile dil in encapsulating resin. We continue to use $\psi = 0°$, $\gamma_0 = 17.2°$, and $D\tau = 0.27$.

After a large amount of arithmetic calculation, one can demonstrate that the ratios $F_{\parallel}^{B}/F_{\parallel}^{C}$ and $F_{\perp}^{C}/F_{\parallel}^{C}$ are quite sensitive to the choice of θ_0 and the pair (θ, θ'). Angle θ' must be chosen to be less than 10°, thereby setting θ at about 27 to 28° to satisfy the dil:encapsulating resin results. What range of θ_0 angles are consistent with the experimental results depends on the proportion of randomly oriented dil. (The meaning of "consistent" here is quite liberal,

[3]Thompson, Nancy, and Daniel Axelrod. Unpublished results.

implying agreement to within ±40% of the central experimental value for each ratio.) In the model where 100% of the dil follows the proposed orientation model, θ_0 must be less than about 12°. In the preferred model where 88% of the dil is well-oriented and the remainder is randomly oriented, θ_0 must be less than about 5°. Instead of assuming that all the bridges form the same angle θ_0 with the surface, we might assume that the bridge orientations are uniformly spread over a range of θ_0 angles averaging 5° at most. Then the maximum θ_0 found for any bridge can be no more than about 10°. In conclusion, the accuracy of the experimental results is sufficient to place the great majority of the dil conjugated bridges within about 10° of parallelism with the surface.

The polarization results presented here, which strongly support the view that dil is incorporated into the bilayer, also suggest an application of similar techniques to problems in liposome-cell fusion. In the interaction between phospholipid vesicles and cells, true fusion must be distinguished from stable adsorption, endocytosis, and lipid transfer (13). Examination of the fluorescence polarization of target cells treated with liposomes containing an oriented fluorescent probe might help to resolve this question.

APPENDIX

High Aperture Correction of Fluorescence Polarization

We must first define two right-handed coordinate systems (Fig. 7): one (the X system) is a microscope-fixed reference frame; the other (the X^0 system) is a nonfixed frame convenient for analyzing the polarization of rays in object space. Both of these systems share the same origin at which is located the transition dipole moments of the fluorescent sample under view in the object space of the objective. We assume for simplicity of units that the adsorption and emission dipole moments are of unit magnitude.

In the X system, X_1 is parallel to the optical axis of the microscope and the X_3 axis is parallel to the electric field vector of the polarized excitation light. An emission dipole has components along these axes denoted by (x_1, x_2, x_3). A typical emitted fluorescence ray propagates toward the objective in a direction given by polar angle, σ, and azimuthal angle, ϕ, with respect to the X_1 and X_3 axes, respectively. Because

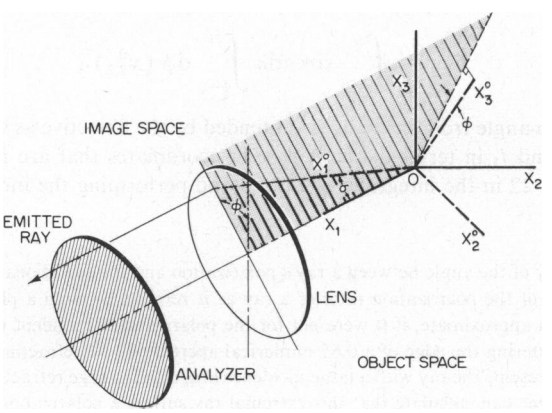

FIGURE 7 Coordinate systems X (microscope-fixed) and X_0 (emitted ray-fixed). The fluorescent sample is at origin O. The meridional plane is shaded. The emitted ray travels along X_1^0 in object space and then parallel to X_1 in image space. Axis X_3 is the direction of the excitation light polarization. Axes X_3 and X_3^0 both make the same angle ϕ with the meridional plane.

the microscope objective's tube length is much larger than its diameter, the fluorescence light ray is refracted into a direction nearly parallel to the optical axis. The ray then passes through an analyzing polarizer filter placed behind the objective in image space.

In the X^0 system, the X_1^0 axis is defined to be along the ray's propagation direction in object space. The X_3^0 axis is chosen as the polarization direction of fluorescence light in object space, which when refracted through the objective into image space, will be parallel to the X_3 axis (i.e., the polarization direction of the excitation light). Assume that the amount of reflection at each surface of the optical system is not large.[4] Then the angle between the polarization direction of an emitted ray and the meridional plane (i.e., the plane containing the path of the ray and the optical axis X_1) must be the same in both object space and image space (14). Because the X_3 axis makes an angle of ϕ with the meridional plane, any ray with polarization parallel to X_3 in image space must have a polarization direction in object space (defined as the X_3^0 direction) at an angle of ϕ with respect to the meridional plane. X_3^0 must also be perpendicular to X_1^0, so these requirements completely determine the orientation of coordinate system X_0. By similar argument, one can show that rays in object space polarized along X_2^0 will be polarized along X_2 in image space.

The rotation matrix transforming coordinates from the X system to the X^0 system can be derived as the product of three successive rotations: a rotation of ϕ around X_1, followed by a rotation of $-\sigma$ around the new X_2, followed by a rotation of $-\phi$ around the newest X_1. Via this transformation, the coordinates of an emission dipole in the X^0 system (x_1^0, x_2^0, x_3^0) are related to its coordinates in the X system (x_1, x_2, x_3) by the rotation matrix equation:

$$\begin{pmatrix} x_1^0 \\ x_2^0 \\ x_3^0 \end{pmatrix} = \begin{pmatrix} \cos\sigma & \sin\sigma\sin\phi & -\sin\sigma\cos\phi \\ -\sin\sigma\sin\phi & \cos\sigma\sin^2\phi + \cos^2\phi & -\cos\sigma\sin\phi\cos\phi + \sin\phi\cos\phi \\ \sin\sigma\cos\phi & -\cos\sigma\sin\phi\cos\phi + \sin\phi\cos\phi & \cos\sigma\cos^2\phi + \sin^2\phi \end{pmatrix} \begin{pmatrix} x_1 \\ x_2 \\ x_3 \end{pmatrix}. \quad (22)$$

Consider the fluorescence from a single emission dipole of components (x_1, x_2, x_3) located at the origin. The fluorescence intensities $I_\perp$ and $I_\parallel$ transmitted through the image space analyzer oriented perpendicular and parallel, respectively, to the excitation polarization direction are (suppressing all multiplicative constants):

$$I_{\perp,\parallel} = \int_{\sigma=0}^{\sigma_0} \sin\sigma d\sigma \int_{\phi=0}^{2\pi} d\phi\, (x_{2,3}^0)^2, \quad (23)$$

where σ_0 is the maximum angle from the X_1 axis subtended by the objective as viewed from the origin.

One can express $I_\perp$ and $I_\parallel$ in terms of the X system coordinates that are fixed with respect to the microscope by using Eq. 22 in the integrand of Eq. 23 and performing the indicated integrations. The

[4]The approximate constancy of the angle between a ray's polarization and the meridional plane results directly from the approximate constancy of the polarization ratio of a ray as it refracts through a planar interface. These rules would be exact, rather than approximate, if it were not for the polarization dependent reflectivity coefficient at an interface. Consider a ray entering the edge of a 0.65 numerical aperture 40 × refracting objective with a flat front surface. This air objective presents the ray with a large incidence angle and a large refractive index change, conditions that maximize reflection. One can calculate that this extremal ray suffers a polarization change of only 6.5% upon transmission past the front surface. Most rays enter at smaller incidence angles and suffer even smaller polarization changes. But even this small worst-case polarization change is unlikely to be encountered in practice because real microscope objectives are coated specifically to suppress reflection. In view of this, one would expect the arguments concerning the constancy of angles made with the meridional plane to be a quite good approximation for all objectives.

result is Eqs. 1 and 2 of Theory section *a*. This result is consistent with that of Dragsten (10), whose derivation follows a different approach involving vector algebra, hypothetical reflection planes, and a constant normalization factor of $(1/2)(1 - \cos\sigma)^{-1}$.

I gratefully thank Dr. Alan Waggoner for his generous gift of diI-C_{18}-(3). I also thank Ms. Shirley A. Mieras and Ms. Connie Barker for typing the manuscript.

This work was supported by the following sources: University of Michigan Rackham Faculty Research Grant; Research Corporation Cottrell Research Grant; and National Institute for Neurological and Communicative Disorders and Stroke grant 1 RO1 NS14565-01.

Received for publication 23 August 1978 and in revised form 17 January 1979.

REFERENCES

1. SIMS, P. J., A. S. WAGGONER, C-H WANG, and J. F. HOFFMAN. 1974. Studies on the mechanism by which cyanine dyes measure membrane potential in red blood cells and phosphatidylcholine vesicles. *Biochemistry.* **13**:3315.
2. WAGGONER, A. S., C. H. WANG, and R. L. TOLLES. 1977. Mechanism of potential-dependent light absorption changes in lipid bilayer membranes in the presence of cyanine and oxonal dyes. *J. Membr. Biol.* **33**:109.
3. ROSS, W. N., B. M. SALZBERG, L. B. COHEN, A. GRINVALD, H. V. DAVILA, A. S. WAGGONER, and C. H. WANG. Changes in absorption, fluorescence, dichroism, and birefringence in stained giant axons: optical measurement of membrane potential. *J. Membr. Biol.* **33**:141.
4. WU, E-S, K. JACOBSON, and D. PAPAHADJOPOULOS. 1977. Lateral diffusion in phospholipid multibilayers measured by fluorescence recovery after photobleaching. *Biochemistry.* **16**:3936.
5. SCHLESSINGER, J., D. AXELROD, D. E. KOPPEL, W. W. WEBB, and E. L. ELSON. 1977. Lateral transport of a lipid probe and labeled proteins on a cell membrane. *Science (Wash. D.C.)* **195**:307.
6. JOHNSON, M., and M. EDIDIN. 1978. Lateral diffusion in plasma membrane of mouse egg is restricted after fertilization. *Nature (Lond.)* **272**:448.
7. AXELROD, D., A. WIGHT, W. WEBB, and A. HORWITZ. 1978. Influence of membrane lipids on acetylcholine receptor and lipid probe diffusion in cultured myotube membrane. *Biochemistry.* **17**:3604.
8. BADLEY, R. A., W. G. MARTIN, and H. SCHNEIDER. 1973. Dynamic behavior of fluorescent probes in lipid bilayer model membranes. *Biochemistry.* **12**:268.
9. YGUERABIDE, J., and L. STRYER, 1971. Fluorescence spectroscopy of an oriented model membrane. *Proc. Natl. Acad. Sci. U.S.A.* **68**:1217.
10. DRAGSTEN, P. 1977. Mechanism of voltage-induced fluorescence changes of the membrane probe merocyanine 540. A fluorescence polarization study. Ph.D. thesis. Cornell University, Ithaca, N.Y.
11. WEBER, G. 1966. Polarization of the fluorescence of solutions. *In* Fluorescence and Phosphorescence Analysis: Principles and Applications. D. M. Hercules, editor. John Wiley & Sons Inc., New York. 217.
12. PETERS, R., J. PETERS, K. H. TEWS, and W. BÄHR. 1974. A microfluorimetric study of translational diffusion in erythrocyte membranes. *Biochim. Biophys. Acta.* **367**:282.
13. PAGANO, R. E., and J. N. WEINSTEIN. 1978. Interactions of liposomes with mammalian cells. *Annu. Rev. Biophys. Bioeng.* **7**:435.
14. RICHARDS, B., and E. WOLF. 1959. Electromagnetic diffraction in optical systems II. Structure of the image field in an aplanatic system. *Proc. R. Soc. Lond. A. Math. Phys. Sci.* **253**:349.